Multiarm spirals in a two-dimensional cardiac substrate

Nenad Bursac*, Felipe Aguel†, and Leslie Tung‡

Department of Biomedical Engineering, Johns Hopkins University, Baltimore, MD 21205

Edited by Harry L. Swinney, University of Texas, Austin, TX, and approved September 16, 2004 (received for review February 11, 2004)

A variety of chemical and biological nonlinear excitable media, including heart tissue, can support stable, self-organized waves of activity in a form of rotating single-arm spirals. In particular, heart tissue can support stationary and meandering spirals of electrical excitation, which have been shown to underlie different forms of cardiac arrhythmias. In contrast to single-arm spirals, stable multiarm spirals (multiple spiral waves that rotate in the same direction around a common organizing center) have not been demonstrated and studied yet in living excitable tissues. Here, we show that persistent multiarm spirals of electrical activity can be induced in monolayer cultures of neonatal rat heart cells by a short, rapid train of electrical point stimuli applied during single-arm-spiral activity. Stable formation is accomplished only in monolayers that show a relatively broad and steep dependence of impulse wavelength and propagation velocity on rate of excitation. The resulting multiarm spirals emit waves of electrical activity at rates faster than for single-arm spirals and exhibit two distinct behaviors, namely ''arm-switching'' and ''tip-switching.'' The phenomenon of rate acceleration due to an increase in the number of spiral arms possibly may underlie the acceleration of functional reentrant tachycardias paced by a clinician or an antitachycardia device.

Rotating single-arm spirals can exist in different chemical (1–4) and biological systems (5–8). If a spiral is stationary or weakly meandering, it represents a persistent source of highly periodic activity with a period of rotation that is determined by the properties of excitation, recovery, and diffusion in the medium. In the heart, stable single-arm spirals can underlie periodic activity such as monomorphic tachycardia, whereas unstable spirals that continuously form and break up are shown to underlie aperiodic and lethal heart activity, namely fibrillation (9). So far, stable rotating structures with a higher degree of organization, such as multiarmed spirals, have been demonstrated experimentally in chemically (2) or light-controlled (10) Belousov–Zhabotinsky reactions, in starving social amoebae *Dictyostelium discoideum* (11), and in FitzHugh–Nagumo-type computer models of homogenous weakly excitable media (12–14). The modes of induction of these multiarmed spirals [i.e., use of an unexcitable central obstacle that is subsequently removed (2, 10) and spontaneous formation from dense multiple wavebreaks (12) or from preset spatial distributions of excited and recovered medium (13, 14)] are not applicable to cardiac tissue. Moreover, healthy cardiac tissue exhibits normal excitability, in contrast to two-variable FitzHugh–Nagumo models, which require weak excitability to support stable multiarm spirals (12–15). In a normally excitable medium, the existence of a stable multiarm spiral as an entity distinct from negligibly interacting adjacent single spirals was questioned by Winfree (16, 17), who considered that in this case distinct rates of rotation are necessary to regard multi- and single-arm spirals as two qualitatively different phenomena.

Here, we show, by optical mapping of electrical activity, the mechanisms of induction and maintenance of stable multiarm spiral waves in normally excitable two-dimensional sheets of heart cells. When compared with single spirals in the same cardiac medium, the multiarm spirals emit slower, narrower, and more frequent waves of activity. They exhibit complex wave dynamics (''arm-switching'' and ''tip-switching'') in the central region, while maintaining stable angular separation between the spiral arms in the periphery. Moreover, we show that accelerated multiarm spirals are favored in a normally excitable heart substrate that exhibits relatively steep steady-state restitution relations.

Materials and Methods

Cell Culture. Confluent anisotropic monolayers made of neonatal rat ventricular cells were cultured on 20-mm-diameter coverslips by using microabrasion methods as described in ref. 18. Special care was taken to ensure a high degree of structural and functional uniformity through the use of visual inspection, electrophysiological measurements during point pacing, or immunofluorescent staining of cardiac and noncardiac cells (18). Average longitudinal and transverse velocities of impulse conduction during pacing at 2 Hz in cultures with multiarm spirals were 26.9 ± 3.1 and 13.3 ± 1.6 cm/s, respectively, yielding average anisotropy ratios (ratio of longitudinal vs. transverse velocity) of 2.1 ± 0.5. Stable multiarm spirals also were induced in three isotropic cultures with an average conduction velocity (CV) of 19.2 ± 1.6 cm/s. These conduction velocities were comparable to those previously found in native neonatal rat ventricles (19).

Optical Mapping and Data Analysis. Transmembrane potentials were recorded in 8- to 10-s episodes with the voltage-sensitive dye RH-237 at 61 hexagonally arranged sites with 2-mm spacing by using methods of contact fluorescence imaging as described in refs. 18, 20, and 21. Wave CV, action potential duration (APD), and wavelength (WL) were measured in the longitudinal and transverse directions at the end of 1 min of point pacing at different rates (2 Hz up to the break frequency, in 0.5 Hz steps) to construct restitution curves (i.e., the dependence of CV, APD, and WL on pacing rate). No alternans (22) of APD or CV was observed. To compare restitutions among different monolayers and computer models (see below), the value at each pacing rate was expressed as a percentage of the value at a basic rate of 2 Hz. These percent restitutions were fitted (average $R^2 > 0.95$) by a line of the form $\%y = -\alpha \times (\text{rate} - 2) + 100$, such that the slope α represented the average percentage drop of a measured parameter (APD, CV, or WL) per unit excitation rate (units, percent per Hz). Percentage restitutions in the longitudinal and transverse directions did not differ significantly and were pooled together.

This paper was submitted directly (Track II) to the PNAS office.

Abbreviations: APD, action potential duration; AS, arm-switching; CV, conduction velocity; PS, phase singularity; TS, tip-switching; WL, wavelength.

*Present address: Department of Biomedical Engineering, Duke University, Durham, NC 27708.

†Present address: Food and Drug Administration, Rockville, MD 20852.

‡To whom correspondence should be addressed at: Biomedical Engineering Department, Johns Hopkins University, 720 Rutland Avenue, Traylor Building, Room 703, Baltimore, MD 21205. E-mail: ltung@bme.jhu.edu.

www.pnas.org/cgi/doi/10.1073/pnas.0400984101

Phase maps and phase singularity (PS) trajectories were constructed by using a time lag of 15 ms (23) from filtered, optically recorded voltage data interpolated to a rectangular mesh with 0.20 × 0.17-mm elements. To evaluate the effect of interpolation, a meandering spiral wave was computer-simulated for 10 s on a finely discretized mesh (see below). PS trajectories were generated from simulated voltage traces at this high spatial resolution and from traces chosen at 61 hexagonally distributed sites by using the interpolation method described above. The two PS trajectories differed on average by only 0.12 ± 0.08 mm. All data are presented as mean or mean ± SD. Comparisons are made by using two-tailed Student's *t* test.

Computer Simulations. The monodomain equation for impulse propagation, $\nabla \cdot G_{si} \nabla V_m = \beta_{sv}(C_m dV_m/dt + I_{ion})$, was solved by using a Galerkin finite element method and a linear triangular discretization with internodal distance of 100 μm (24). For validation of the interpolation method, a meandering spiral wave was simulated on a 20-mm circular substrate by using the Karma action potential model (25). For plots of the APD and CV restitutions, FitzHugh–Nagumo-type models (12, 13) were simulated on a 0.5- × 20-mm tissue strip. The strip was stimulated at one end at progressively higher rates (2 Hz up to break frequency, in 1-Hz steps), APDs and CV were recorded between two points at the other end of the strip, and normalized restitution curves were plotted and fitted as described above. Parameters of the monodomain equation were $dt = 0.01$ ms, $G_{si} = 0.1$ S/m, $\beta_{sv} = 140{,}000$ m^{-1}; $C_m = 1$ μF/cm^2; parameters from ref. 25 were $M = 4$, $R_e = 0.5$, and $\tau_E = 20$; parameters from ref. 13 were $C_2 = 0.75$; and parameters from ref. 12 were $a = 0.05$ and $k = 4.86$. Equations and values of other parameters are given in *Computational Methods* and Table 1 (which are published as supporting information on the PNAS web site) and were the same as in the respective references.

Results and Discussion

We cultured confluent, normally excitable sheets (monolayers) of neonatal rat heart cells (18, 21) and induced a single-arm spiral (functional reentry) by applying a rapid (5–6 Hz) burst of 10–20 pulses at 1.2× threshold from a point electrode in the center of the monolayer. The average rate of rotation of single-arm spirals was 4.6 ± 1.2 Hz ($n = 75$ monolayers). The center of rotation (referred to hereafter as "tip") of the spiral wave can be described mathematically as a PS point where all phases of the action potential converge together at one point in space (23). The phase maps and space-time plots of PS trajectories (Fig. 1*A* and see also Fig. 3*C*) reveal the dynamics of spiral wave formation, annihilation, and tip motion. During single-arm spiral activity, 3–15 cathodal point stimuli (1.2× threshold, at a 10–40% higher rate than that of the single spiral) were applied at an arbitrary position on the periphery of the cell culture, 6.3 ± 1.4 mm away from the center of the rotating spiral, causing a transient formation of pairs of short-lived wavelets (23) and an increase in the number of phase singularities (multiplication) (Fig. 1*A*). In the majority of cases (64 of 75 monolayers), all of the multiplied waves were annihilated in mutual collisions or against the boundary of the monolayer, resulting in the termination of single-spiral activity. In 11 of 75 monolayers, two or three rotating waves with the same chirality (direction of rotation) as that of the original spiral survived after pacing (Fig. 1*A* and see also Movie 1, which is published as supporting information on the PNAS web site, for the successful two-arm initiation) and within two rotations became locked with ≈180° circumferential separation to form a stable two-arm spiral (21 episodes in 9 monolayers) (Fig. 2*A*) or ≈120° separation to form a three-arm spiral (5 episodes in 2 monolayers) (Fig. 2*B* and Movie 2, which is published as supporting information on the PNAS web site), respectively. The spiral arms steadily rotated at the same frequency and excited heart cells periodically (with variation <2%) at a rate faster than that of the original spiral (Fig. 1*B*). The same rotational frequency is crucial for the coexistence and stability of multiple spiral arms; otherwise, the spiral with the highest frequency would dominate and override all other spirals, at least in a homogeneous medium (26). Over time, the

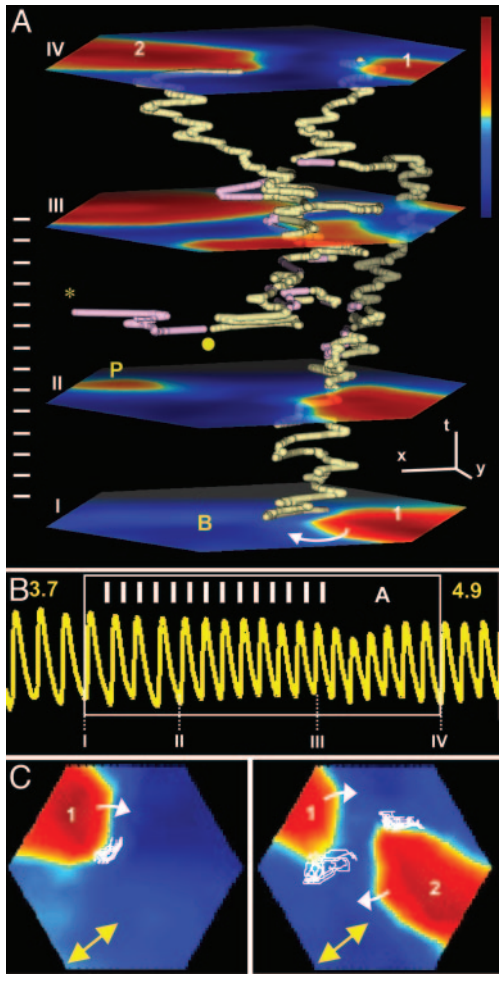

Fig. 1. Initiation of a double-arm spiral in a cultured cardiac monolayer (see Movie 1). (*A*) Transmembrane voltage (fluorescence) was measured optically from a hexagonal area of monolayer with 8.5-mm edge and color-coded from blue (rest) to red (fully depolarized). Planes I–IV show voltage snapshots at four points in time. Motions of spiral wave tips (i.e., centers of wave rotation) are represented by PS trajectories in x, y, and t space (23). PS with clockwise and anticlockwise chirality are shown in yellow and purple, respectively. A clockwise single-arm spiral (labeled 1 on plane I) is paced by a pulse train (white bars on the left) at a point on the monolayer periphery (labeled P on plane II). During pacing (planes II and III), new waves of opposite chirality form in pairs (●) and annihilate either by merging in pairs or colliding individually against the monolayer boundary (*). After pacing terminates, two spirals having the same chirality as the initial spiral survive and form a stable two-arm spiral (plane IV, arms labeled 1 and 2). (x, y, and t bars are 2 mm, 2 mm, and 300 ms, respectively.) (*B*) A 5.4-s voltage trace from a site labeled B in the bottom plane in *A*. White frame denotes trace during *A*. Numbers I–IV denote the times of voltage snapshots (planes) from *A*. Multiplication of arms (from 1 to 2) accelerates the rate of cell firing from 3.7 to 4.9 Hz. (*C*) PS trajectories (white lines) in the plane of monolayer during 2-s rotation, before (*Left*) and after the formation (shown in *A*) of stable two-arm spiral (*Right*). Note that PS trajectories generally follow the longitudinal direction of anisotropy (indicated by double-headed arrow).

PHYSIOLOGY

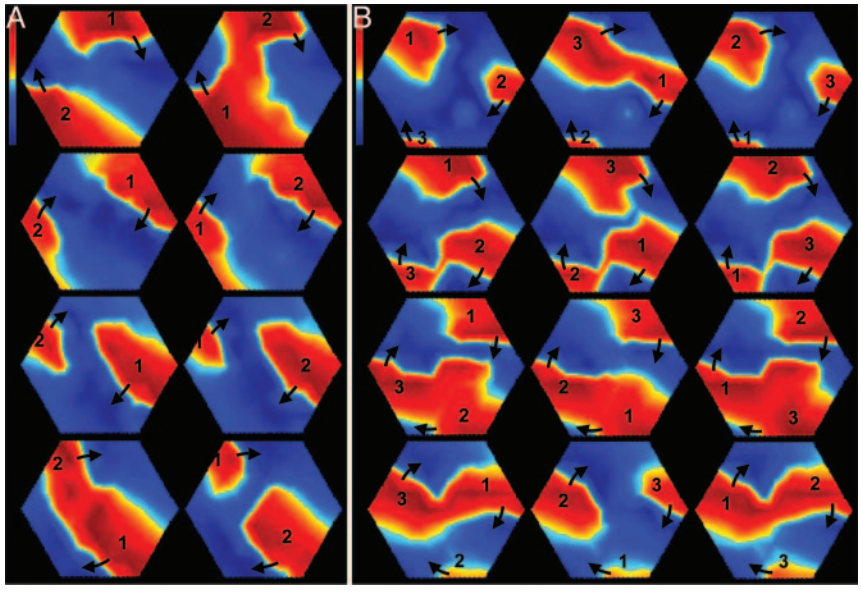

Fig. 2. Stable two-arm (*A*) and three-arm (*B*) (see Movie 2) spirals in cardiac monolayers. Transmembrane voltage (fluorescence) is coded from blue to red. Frames read columnwise, left to right, and span one full rotation of each arm. Time between frames is 50 ms in *A* and 45 ms in *B*. Each arm is labeled by number, and wavefront direction is indicated by arrows. Spiral arms rotate at the same frequency, interact in a complex fashion in the central zone, and maintain a separation of ≈180° (two-arm) or ≈120° (three-arm) in the periphery. Note that spiral arms are short in length due to the relatively small size of the cardiac monolayer compared with the WL of propagated waves.

arms appeared to alternatively repel and collide in a complex fashion in the central zone (between the arm tips), while maintaining their circumferential relationship in the periphery (Fig. 2). Cardiac cells in the central zone were excitable, often exhibited action potentials with electrotonic humps, and fired at rates equal to or lower than the cells in the periphery (Fig.

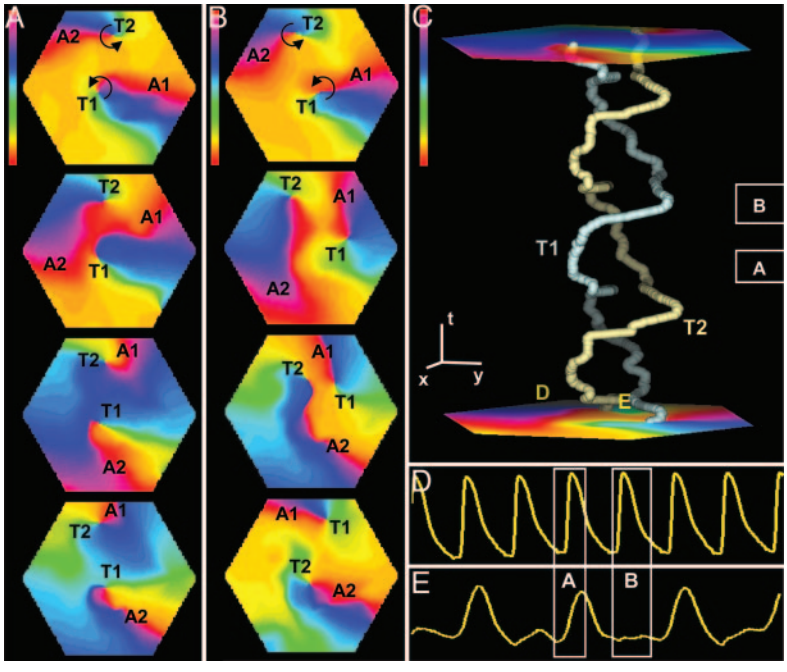

Fig. 3. Interactions between two corotating spiral arms in cardiac monolayers. Phase snapshots reveal two scenarios, AS (*A*) and TS (*B*). Initially (top frames), each arm (A1, A2) and its tip (T1, T2) have the same index number (T1-A1 and T2-A2 pairs). During AS, arms collide in the center and switch to the other tip (forming T1-A2 and T2-A1 pairs). During TS, tips (phase singularities) drift and switch position, while arms do not collide (T1-A1 and T2-A2 pairs remain intact). Time between frames is 40 ms in *A* and 50 ms in *B*. (*C*) Tip (T1, T2) trajectories during 1.5 s of the same two-arm spiral. Repetitive alternations of TS and AS in this case produce a helical pattern in a space–time plot. In the *x-y* plane (cell monolayer plane), the tips traverse virtually the same closed path (data not shown). (x, y, and t bars are 2 mm, 2 mm, and 150 ms, respectively) (Color bars in *A*–*C* are $-\pi$ to π.) *D* and *E* are voltage traces at sites far from tips (periphery) and between tips (central zone), respectively, as marked by D and E in the bottom plane of *C*. White frames in *C*–*E* denote the same time intervals as during *A* and *B*. During AS (A), cells fire in both the central zone and periphery, whereas during TS (B), conduction is blocked in the central zone. Alternating AS and TS in this case corresponds to a 2:1 propagation block in the central zone (*E*).

3 *D* and *E*). Once initiated, the multiarm spirals stably persisted until their disruption by external pacing (usually performed 10–30 min after initiation).

Phase maps revealed two distinct types of interaction between spirals of the same chirality: ''arm-switching'' (AS), in which the depolarization fronts of spiral arms interact and arms switch between tips that stay relatively stationary (Figs. 3*A* and 1*C Right*), or ''tip-switching'' (TS), in which tips drift in the direction of spiral rotation and switch positions without any separation of, or interaction between, their respective arms (Fig. 3*B*). Waves collided and cells fired in the central zone during AS, whereas propagation was blocked and cells were unexcited in the central zone during TS (Fig. 3 *D* and *E*). An equivalent of persistent AS was demonstrated previously in experimental studies in light-controlled chemical reactions (10), and an equivalent of persistent TS was described in computational studies by Vasiev *et al.* (12). In our study, 11 episodes (5 monolayers) of multiarm spirals involved persistent AS, 15 episodes (6 monolayers) involved both AS and TS, and no episodes involved persistent TS. This result is in agreement with the analytical and numerical studies of Hakim and Karma (27), who showed that rotation of multiple spirals around a common excitable, but unexcited, core (an equivalent of persistent TS) is linearly unstable in weakly excitable media (including ref. 12) and that spirals eventually invade the excitable core, collapse, and yield AS. In cardiac cultures where AS and TS occurred, each TS was followed by at least one AS, such that the firing rate in the central zone was between 50% and 100% of the rate in the periphery (Fig. 3*C*).

The tip trajectory (Fig. 1*C*) during a full rotation of one arm in a multiarm spiral was longer than that for the single-arm spiral in the same medium (15.4 ± 4.4 mm vs. 10.3 ± 2.4 mm, $P < 0.001$), whereas the average tip velocities were comparable. This phenomenon rendered the period of one arm in the multiarm spiral (two-arm, 458 ± 35 ms; three-arm, 565 ± 40 ms) to be longer ($P < 0.005$ for both comparisons) than that of the single-arm spiral (319 ± 42 ms). However, in spirals with multiple arms, each site in the periphery was activated multiple times during a single period, yielding an overall rate of activity that was higher than in spirals with just a single arm. This rate acceleration of 38.1 ± 10.0% and 64.2 ± 7.1% in two- and three-arm spirals, respectively ($P < 0.001$ for both comparisons) was accompanied by an average decrease of APD, wave CV, and WL (WL = APD × CV) to between 84% and 76%, 75% and 63%, and 67% and 51% of the initial values, respectively ($P < 0.01$ for all comparisons). Thus, at a site in a cardiac medium far from the central zone, the multiarm spiral is viewed as a source of more frequent but slower and narrower waves compared with a single-arm spiral.

Before the initial induction of single-arm spirals, the steady-state dependences of APD, CV, and WL on rate of excitation were measured in each monolayer (Fig. 4 *A–C*). The cardiac monolayers with inducible multiarm spirals (11 of 75 monolayers) exhibited steeper restitutions (faster decay with rate increase) vs. those spirals (64 of 75 monolayers) where only a single-arm spiral and no acceleration could be induced (average $\alpha = 12.0$ vs. 6.8%, 9.2 vs. 2.9%, and 17.6 vs. 8.4% per Hz for APD, CV, and WL restitutions, respectively; $P < 0.001$ for all comparisons) (Fig. 4). Apparently, the largest difference was in the rate dependence of CV restitution, which is an indirect measure of recovery of medium excitability (17). In our studies, normal excitability of the cardiac medium was dynamically decreased during single-arm spiral activity by wavefront propagation in the wake of refractory tissue. The rapid point pacing at higher rates further decreased excitability and favored the conditions for creating bound spiral waves (12–14). The stable multiarmed spiral with accelerated rate that eventually was formed maintained the additional decrease

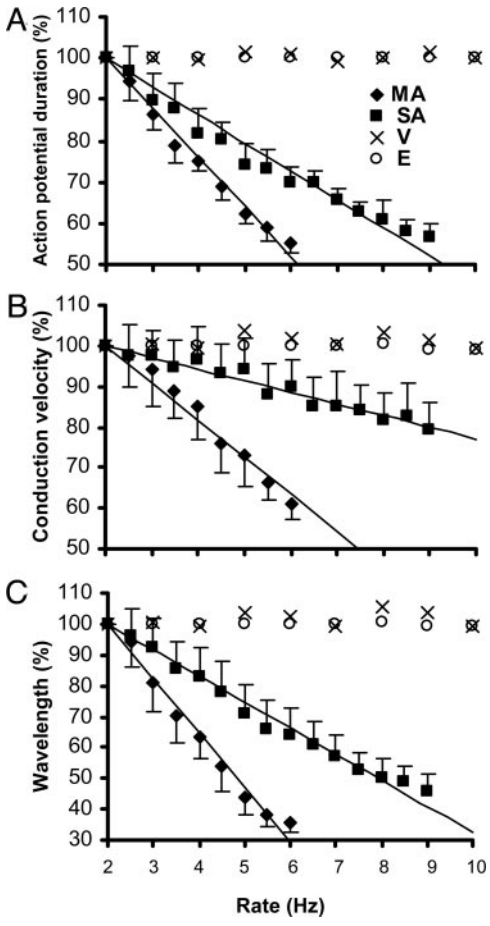

Fig. 4. Steady-state rate dependences of percentage APD (*A*), CV (*B*), and WL (*C*) in cardiac monolayers (filled symbols) and computer models (open symbols). Cultures of neonatal rat myocytes where only single-arm spirals and no acceleration could be induced ($n = 64$) are denoted by ''SA,'' and those with inducible multiarm spirals ($n = 11$) are labeled ''MA.'' A FitzHugh–Nagumo-type computer model with inducible multiarm spirals by Vasiev (12) with $k = 4.86$ is denoted by ''V,'' and a model by Ermakova *et al.* (13) with $C_2 = 0.75$ is denoted by ''E.'' (See *Computational Methods* for details). Data are linearly fit by using the expression % $y = -\alpha \times (x - 2) + 100$. For computer models, α is not significantly different from 0, and linear fit is not shown.

in excitability, yielding lower wavefront curvature, longer tip trajectory, and slower rotation of the spiral arms compared with those of a single-arm spiral in the same medium. In general, steeper restitution relations favor the occurrence of multiarm spirals in a bounded medium because at high activation rates, excitability of the medium is lower, which unwinds the spirals and enables interaction between the tips, and WL is shorter, which facilitates the coexistence of multiple waves in the relatively small area such as in our cardiac cell cultures.

As shown in Fig. 4, FitzHugh–Nagumo-type computational models that were used previously to study multiarm spirals (12, 13) exhibit virtually no dependence of APD, CV, and WL on the rate of excitation and, thus, require a relatively large medium with low excitability to support accelerated multiarm spirals. In contrast, stable multiarm spirals can be sustained in normally excitable and relatively small cardiac cultures by the significant decrease of excitability and WL at increased excitation rates. Therefore, models of cardiac tissue that incorporate appropriate rate dependence of excitability and refractoriness [e.g., full-scale cardiac ionic models (28) or possibly three- or four-variable simplified models (29, 30)] are needed to study experimental

PHYSIOLOGY

phenomena with complex dynamics such as accelerated multiarm spirals.

It is important to note that multiarm spirals in the confluent cardiac cultures, described in this study, are qualitatively a different phenomenon from the pacing-induced "double-wave reentry" shown in rings of cardiac tissue (31, 32), where two waves rotate in the same direction around a common (relatively large) anatomical obstacle. The multiplied spirals described in this study may underlie pacing-induced acceleration (33) of reentrant tachycardias, which are the result of a wave rotating around a functional block (34, 35) rather than an anatomical obstacle. This acceleration, if sufficiently high, may result in further wavebreaks due to the presence of structural or functional heterogeneities in the heart (9), and/or dynamic instability of APD (36), and yield unorganized, incompetent heart activity (fibrillation).

This work was supported in part by a fellowship from the Mid-Atlantic Affiliate of the American Heart Association (to N.B.) and by National Institutes of Health Grant HL66239 (to L.T.).

1. Winfree, A. (1972) *Science* **175,** 634–636.
2. Agladze, K. I. & Krinsky, V. I. (1982) *Nature* **296,** 424–426.
3. Vanag, V. K. & Epstein, I. R. (2001) *Science* **294,** 835–837.
4. Ertl, G. (1991) *Science* **254,** 1750–1755.
5. Lechleiter, J., Girard, S., Peralta, E. & Clapham, D. (1991) *Science* **252,** 123–126.
6. Tomchik, K. J. & Devreotes, P. N. (1981) *Science* **212,** 443–446.
7. Davidenko, J. M., Pertsov, A. V., Salomonsz, R., Baxter, W. & Jalife, J. (1992) *Nature* **355,** 349–351.
8. Witkowski, F. X., Leon, L. J., Penkoske, P. A., Giles, W. R., Spano, M. L., Ditto, W. L. & Winfree, A. T. (1998) *Nature* **392,** 78–82.
9. Jalife, J. (2000) *Annu. Rev. Physiol.* **62,** 25–50.
10. Steinbock, O. & Muller, S. (1993) *Int. J. Bifurcation Chaos* **3,** 437–443.
11. Siegert, F. & Weijer, C. J. (1995) *Curr. Biol.* **5,** 937–943.
12. Vasiev, B., Siegert, F. & Weijer, C. (1997) *Phys. Rev. Lett.* **78,** 2489–2492.
13. Ermakova, E. A., Pertsov, A. M. & Shnol, E. E. (1989) *Physica D* **40,** 185–195.
14. Zaritski, R. M. & Pertsov, A. M. (2002) *Phys. Rev. E* **66,** 066120.
15. Ermakova, Y. A. & Pertsov, A. M. (1986) *Biophysics* **31,** 932–940.
16. Winfree, A. T. (2001) *The Geometry of Biological Time* (Springer, New York), pp. 331, 488–489.
17. Winfree, A. T. (1991) *Physica D* **49,** 125–140.
18. Bursac, N., Parker, K. K., Iravanian, S. & Tung, L. (2002) *Circ. Res.* **91,** e45–e54.
19. Bursac, N., Papadaki, M., Cohen, R. J., Schoen, F. J., Eisenberg, S. R., Carrier, R., Vunjak-Novakovic, G. & Freed, L. E. (1999) *Am. J. Physiol.* **277,** H433–H444.
20. Entcheva, E., Lu, S. N., Troppman, R. H., Sharma, V. & Tung, L. (2000) *J. Cardiovasc. Electrophysiol.* **11,** 665–676.
21. Iravanian, S., Nabutovsky, Y., Kong, C. R., Saha, S., Bursac, N. & Tung, L. (2003) *Am. J. Physiol.* **285,** H449–H456.
22. Pastore, J. M., Girouard, S. D., Laurita, K. R., Akar, F. G. & Rosenbaum, D. S. (1999) *Circulation* **99,** 1385–1394.
23. Gray, R. A., Pertsov, A. M. & Jalife, J. (1998) *Nature* **392,** 75–78.
24. Vigmond, E. J., Aguel, F. & Trayanova, N. A. (2002) *IEEE Trans. Biomed. Eng.* **49,** 1260–1269.
25. Karma, A. (1994) *Chaos* **4,** 461–472.
26. Xie, F., Qu, Z., Weiss, J. N. & Garfinkel, A. (1999) *Phys. Rev. E Stat. Phys. Plasmas Fluids Relat. Interdiscip. Top.* **59,** 2203–2205.
27. Hakim, V. & Karma, A. (1999) *Phys Rev E Stat. Phys. Plasmas Fluids Relat. Interdiscip. Top.* **60,** 5073–5105.
28. Luo, C. & Rudy, Y. (1994) *Circ. Res.* **74,** 1071–1096.
29. Fenton, F. H. & Karma, A. (1998) *Chaos* **8,** 20–47.
30. Fenton, F. H. & Cherry, E. M. (2002) *Chaos* **12,** 852–892.
31. Brugada, J., Boersma, L., Kirchhof, C., Brugada, P., Havenith, M., Wellens, H. J. & Allessie, M. (1990) *Circulation* **81,** 1633–1643.
32. Frame, L. H., Rhee, E. K., Bernstein, R. C. & Fei, H. (1996) *J. Am. Coll. Cardiol.* **28,** 137–145.
33. Fries, R., Heisel, A., Kalweit, G., Jung, J. & Schieffer, H. (1997) *Pacing Clin. Electrophysiol.* **20,** 198–202.
34. Schalij, M. J., Boersma, L., Huijberts, M. & Allessie, M. A. (2000) *Circulation* **102,** 2650–2658.
35. Dillon, S. M., Coromilas, J., Waldecker, B. & Wit, A. L. (1993) *J. Cardiovasc. Electrophysiol.* **4,** 393–411.
36. Garfinkel, A. & Qu, Z. (2000) in *Cardiac Electrophysiology: From Cell to Bedside*, eds. Zipes, D. P. & Jalife, J. (Saunders, Philadelphia), pp. 315–320.